Pressure and Temperature Transient Analysis of Geothermal wells with low permeability

Jorge Alberto Rangel-Arista[1]*, Sadiq J. Zarrouk[1], Eylem Kaya[1] and Katie McLean[2]

[1]Department of Engineering Science, University of Auckland, Private Bag 90210, Auckland, New Zealand

[2]Contact Energy Ltd, Wairakei Power Station, Taupo, New Zealand.

*jran489@aucklanduni.ac.nz

Keywords: *Geothermal, well testing, Pressure transient analysis, Temperature transient analysis, low permeability.*

ABSTRACT

Geothermal well testing is performed during completion activities. The test provides insight into the wellbore and reservoir properties, such as permeability, skin factor, skin radius, boundaries, and faults. Traditionally, the analyses are performed with a focus primarily on pressure transients, potentially overlooking valuable information in the temperature transient, which can improve predictive models. This study analyses pressure and temperature transients of two sets of geothermal well test data with low permeability. By adding the temperature analysis, this study aims to examine the temperature behaviour and enhance the reliability of well-test analysis by considering the contribution of temperature analysis. The results show that the temperature response is related to the reservoir's permeability and the wellbore temperatures. At the same time, the pressure can stabilise even when the temperature remains transient.

1. INTRODUCTION

During completion activities, the injection-falloff test is commonly used to evaluate wellbore and reservoir properties (Zarrouk and McLean, 2019). The sensor (PTS) tool measures pressure, temperature, and spinner velocity (flow) along the wellbore during this test.

Conventional geothermal well testing focuses on pressure transient analysis (PTA), which uses the pressure response to injection flow during an injection-falloff test (Grant and Bixley, 2011; Zarrouk and McLean, 2019). However, the temperature transient analysis (TTA) during the test is neglected.

Some studies do consider the TTA during PTA. However, these studies have mainly focused on oil and gas reservoirs (petroleum industry), such as Dawkrajai et al. (2005), who introduced a wellbore-reservoir model to estimate the pressure and temperature in horizontal wellbores for single and multiphase (water, oil and gas), considering steady-state conditions. Sui et al. (2008) worked on a wellbore-reservoir numerical model, utilising the heat source/sink concept and the overall heat transfer coefficient to couple the wellbore and reservoir response. Silva Junior et al. (2012) proposed a numerical model for vertical smart wells under non-isothermal conditions, dividing them into segments according to the control valves that connect the annular and tubing zones. Ramazanov and Parshin (2006) introduced a set of approximate analytical equations for multiphase fluid flow, assuming a reservoir saturated with oil and water, including oil degassing. Panini and Onur (2018) introduced analytical solutions, decoupling pressure from temperature and using Bolztman transformation and Ramey's (1970) pressure solutions for the skin and formation zones.

In the geothermal industry, Onur and Palabiyik (2015) introduced an analytical model for constant-rate production tests, considering a liquid single phase in a geothermal reservoir with infinite-acting radial flow. McLean and Zarrouk (2017) introduced a numerical geothermal framework to examine the pressure and temperature responses. Adiputro et al. (2020) investigated geothermal wells with water hammer during the injection falloff test, utilising a multilayer numerical model to examine the pressure and temperature responses. Rangel-Arista et al. (2022) modified McLean and Zarrouk's (2017) framework to investigate the temperature response, considering an artificial Peclet number encompassing the multiple heat transfer interactions between the wellbore and reservoir.

It is worth mentioning that a petroleum reservoir is a closed system (no recharges) in which the perforated interval targets oil or gas chambers (Iyengumwena et al., 2013). A geothermal reservoir is an open system (recharges) with a perforated liner ranging from hundreds to thousands of meters (Zarrouk and McLean, 2019).

From the above, the combined analysis of geothermal PTA and TTA is a relatively new field due to the fundamental differences between petroleum and geothermal reservoirs. Therefore, this paper examines the temperature and pressure responses from two geothermal well tests (TH017 and WK684) with low permeability and, hence, slow temperature responses, focusing on the non-isothermal effects.

2. WELL TH017

Well TH017 is located in the Tauhara geothermal field in New Zealand. Its casing design encompasses the surface casing (20"), anchor casing (13 3/8"), production casing (9 5/8"), and open hole (8 1/2") with a perforated liner (7") (Figure 1). The 9 5/8" casing shoe is set at a depth of 1096 m, while the 7" liner extends from 582 to 1983 m (Figure 1). After the 7" liner, there is an open section without liner, covering the last 256 m to the total depth of 2236 m.

2.1. Injection/falloff test

During the completion tests, the pressure, temperature and spinner (PTS) sensor tool remained at a depth of 1500 m while the injection flow rate was controlled at the ground surface (Figure 2). In the first 47602 s, the injection flow rate varied between 0 and 7.2 kg/s. During this period, the sensor tool remained on the ground surface (Figure 2).

ISSN 2703-4275

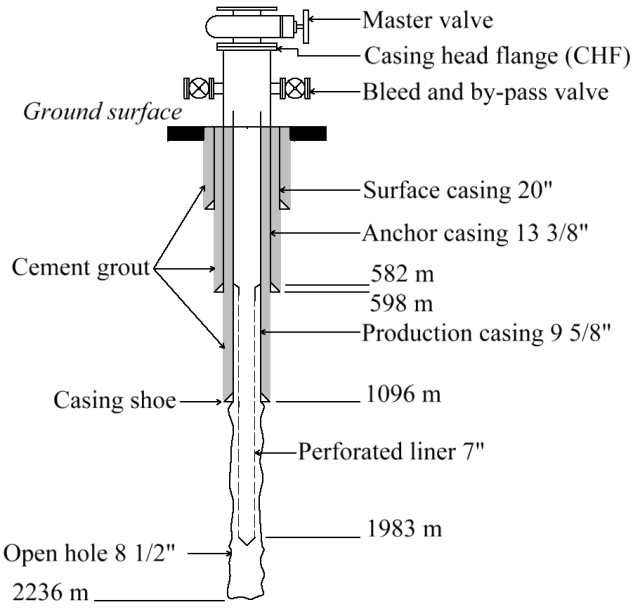

Figure 1: Well TH017 casing design.

At 47603 s, the PTS tool traveled downward, reaching the 1930 m depth at 52131 s (Figure 2, Point A). Simultaneously, a new injection step started (6.25 kg/s). The pressure and temperature varied during this period because of the sensor tool movement (Figure 2).

Next, the PT tool ascended and descended, reaching the target depth of 1500 m at 55671 s (Figure 2, Point B). The injection flow rate rose to 37.8 kg/s (52200 s) during this period. Afterwards (>55671 s), the sensor tool remained at the target depth (1500 m) for a period of 17034 s (Figure 2, Point C).

The injection flow rate changed during this time: 41.52, 51, 63.4, 0, 58.59, 74, 71, 6.5 and 7.5 kg/s. In response to the injection flow steps, the pressure and temperature built up and fell off (Figure 2).

At 72705 s (Figure 2, Point C), the sensor tool moved along the wellbore up to 89055 s (Figure 2, Point D). The injection flow experienced three increasing steps (7.5, 25.4 and 38 kg/s).

The sensor tool (Figure 2, Point C – Point D) generated pressure, temperature and spinner velocity profiles during each increasing flow step (Figure 3). The pressure profiles during the three increasing injection steps (7.5, 25.4 and 38 kg/s) are parallel (Figure 3), indicating poor permeability. As the injection flow rate rose from 7.5 to 38 kg/s, the pressure increased, obtaining the greatest pressure at the highest injection step (38 kg/s) (Figure 3).

The temperature profiles (Figure 3) showed an almost constant temperature with slight fluctuations before the 1200 m depth during the three injection steps (7.5, 25.4 and 38 kg/s). The injection steps prompted a cooling effect that is more predominant inside the casing because of the lack of interaction between the wellbore and reservoir.

After the 1200 m depth (Figure 3), the three temperature profiles show a sharp, short increase at 1210, 1382, 1505 and 1908 m. These sharp, short temperature rises indicate possible feed zones (Figure 3, yellow bands). In particular, after the 1515 m depth, the temperature profiles show a linear rise until they experience a short, sharp temperature increase at different depths, indicating possible feed zones. At 1590 m depth, the 7.5 kg/s injection step temperature profile reached 118°C. At 1650 m depth, the 25.4 kg/s injection step temperature profile reached 122.2°C. At 1770 m depth, the 38 kg/s injection step temperature profile reached 133.15°C (Figure 3, yellow band).

The fluid velocity profiles show similar trends in different periods (Figure 3). The velocity profiles show fluctuating positive values inside the casing production (<1096 m depth). After 1096 m depth, the velocities decrease significantly for the three injection steps (38, 25.4 and 7.5 kg/s). These velocity drops represent a feed zone from 1096 to 1140 m depth (Figure 3, yellow band).

Next (>1140 m), the velocity profiles show short, sharp drops at 1210 (injection steps: 7.5, 25.4 and 38 kg/s), 1505 (injection steps: 25.4 and 38 kg/s) and 1627 m (injection step: 38 kg/s) (Figure 3). These velocity drops show possible feed zones, which the temperature profiles confirmed through the sharp, short increase (Figure 3, yellow bands). In particular, after the 1140 m, the velocity fluctuations are minor because most of the injected fluid entered the feed zone located between 1096 and 1140 m.

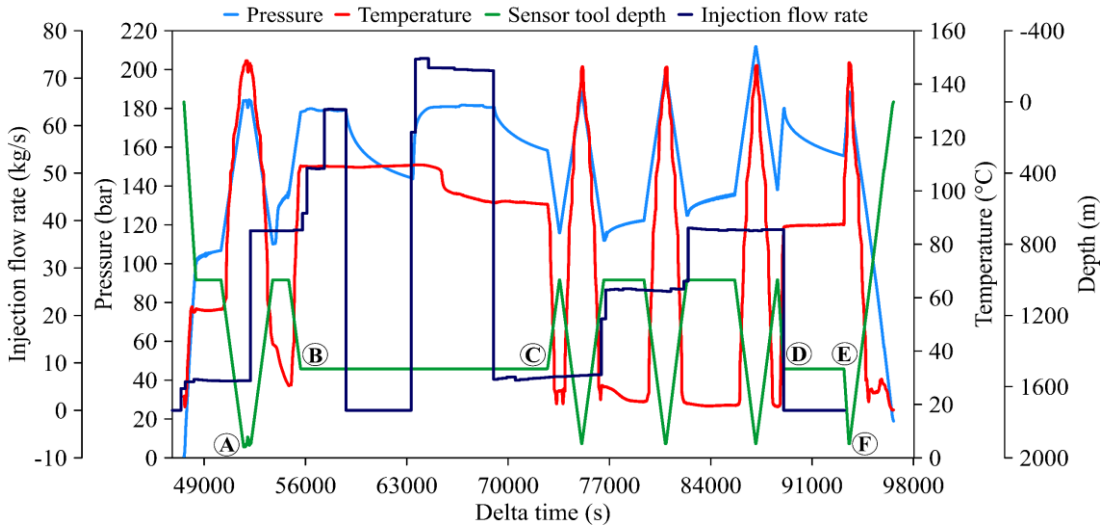

Figure 2: Well TH017 injection/falloff test.

ISSN 2703-4275

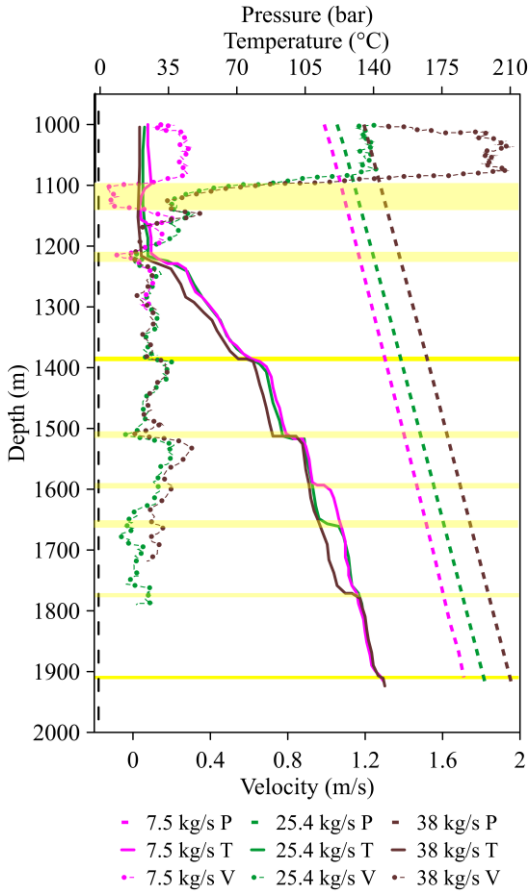

Figure 3: Well TH017 injection steps: pressure (P), temperature (T) and fluid velocity (V) profiles.

The temperature and velocity profiles (Figure 3, yellow bands) identified eight possible feed zones (Table 1). The most significant feed zone runs from 1096 to 1140 m depth.

After the sensor tool recorded the pressure, temperature and spinner velocity (Figure 3) during the three increasing injection steps (Figure 2, Point C – Point D), it reached the target depth of 1500 m at 89055 s (Figure 2, Point D) and remained at this location. Simultaneously, the injection step changed from 38 to 0 kg/s, reflecting the beginning of the pressure falloff period (Figures 2b and 4).

During the falloff period (Figure 4), the pressure drops from 180 to 155.64 bar in 4140.25 s without reaching the initial pressure, indicating low formation permeability (Zarrouk and McLean, 2019). During the same time, the temperature shows a minor buildup from 86.49 to 87.39°C (ΔT ~0.9°C) with minor fluctuations (Figure 4), supporting the presence of low permeability because there is a lack of hot fluid flowing from the reservoir into the well.

After the pressure falloff period ends (Figure 2, Point E), the sensor tool travels downward to pass the test target to tag the deepest point of the well, which is a common practice in well testing (Zarrouk and McLean, 2019). In this case, the sensor tool only reaches 1958 m (Figure 2, Point F) before the perforated liner ends (Figure 1). Then, it travels upward to the ground surface. During this time, the pressure and temperature change because of the sensor tool depth variation (Figure 2). The well TH017 test lasted 96626 s (26.84 hours).

Table 1: Possible well TH017 feed zones.

Depth		Feed zone
From	To	
1096	1140	Yes
1140	1210	No
1210	1225	Yes
1225	1382	No
1382	1390	Yes
1390	1505	No
1505	1515	Yes
1515	1590	No
1590	1598	Yes
1598	1650	No
1650	1662	Yes
1662	1770	No
1770	1780	Yes
1780	1908	No
1908	1912	Yes
1912	2240	No

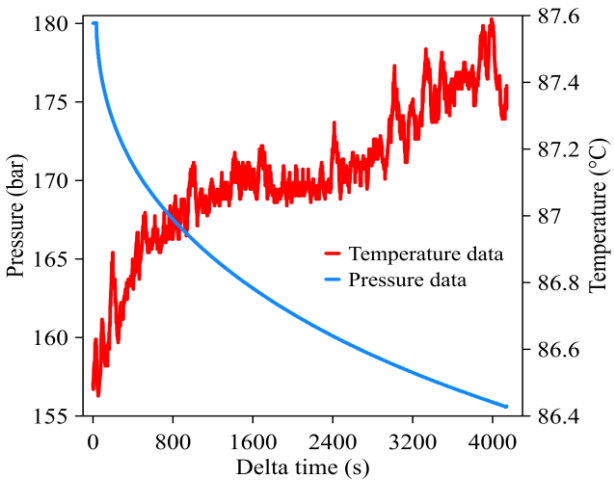

Figure 4: TH017 pressure falloff period: Pressure and temperature.

TH017 showed an actual injectivity index (II) of 1.61 tonne/h/bar and an apparent injectivity of 23.74 tonne/h/bar (Figure 5). We employed the downhole pressure to estimate the II, as the wellhead pressure (WHP) measurements are unavailable. The apparent injectivity (Figure 5, golden dots) shows multiple points for the same flow rate, making the linear fit look unsuitable.

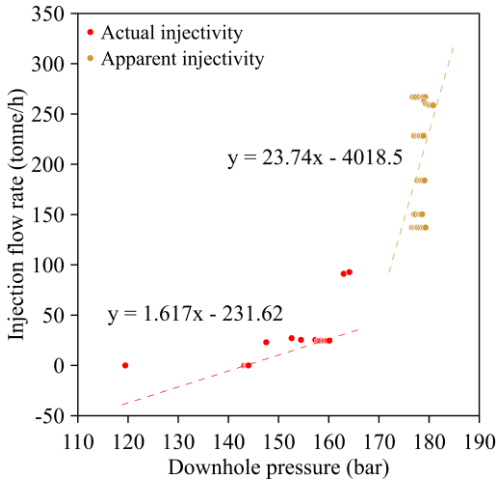

Figure 5: Well TH017 injectivity index (II).

2.2. Heat-up tests

During the heat-up test, the PT tool recorded the pressure and temperature profiles at 1 hour, 1.5 days, 7 days and 28 days after the injection test (Figure 6). The pressure decreases during the heat-up test, changing from 186.5 bar (1-hour heat-up test at 1909.1 m depth) to 151.48 bar (28 days heat-up test at 1909.1 m depth). As the pressure stabilises over time, the well water level decreases from the ground surface (1-hour heat-up test) to ~91 m depth (28-day heat-up test) (Figure 6).

The parallel pressure profiles show no pressure control point (PCP) and low permeability because of a weak link between the reservoir and the wellbore (Zarrouk and Mclean, 2019).

The 1-hour heat-up profile (Figure 6, orange line-solid circles) shows slight fluctuations between 17.69°C and 29.49°C until 1216 m depth. Then (>1216 m depth), the temperature experiences a short, rapid increase for the next 14 m, reaching a temperature of 44.66°C. This temperature behaviour (Figure 6, yellow band) reinforces the existence of a feed zone previously observed in the spinner and temperature profiles during the injection test (Figure 3).

Then (>1230 m depth), the 1-hour temperature profile shows short, sharp rises at 1383, 1510, and 1765 m depth, meaning the existence of feed zones (Figure 6, yellow band), which we identified along the injection test (Figure 3, yellow bands). Finally, the 1-hour temperature profile reaches 147.47°C at 1919.5 m depth (Figure 6, orange line).

The 1.5-day, 7-day, and 28-day temperature profiles show similar trends with gradual stabilisation over time (Figure 6). The temperature remains almost constant in the first meters for the three heat-up tests before the sensor tool reaches the well water level. Then, the temperature profiles rise, forming a hump and reaching 76.69°C (1.5-day heat-up test at 525.42 m depth), 101.12°C (7-day heat-up test at 538.14 m depth), and 115.45°C (28-day heat-up test at 533.9 m depth) (Figure 6). Then, the temperature profiles drop and fluctuate until 1210 m depth.

Afterwards, the temperatures show a brief, sharp increase in the next 30 m because of a feed zone (Figure 6, yellow band). This zone (1210 m – 1240 m depth) coincides with the feed area detected by the velocity profile (Figure 3, yellow band). The temperature profiles reach a final temperature of 155.9°C at 1928 m depth (1.5-day heat-up test), 161.8°C at 1932.2 m depth (7-day heat-up test), and 167.7°C at 1902.5 depth (28-day heat-up test).

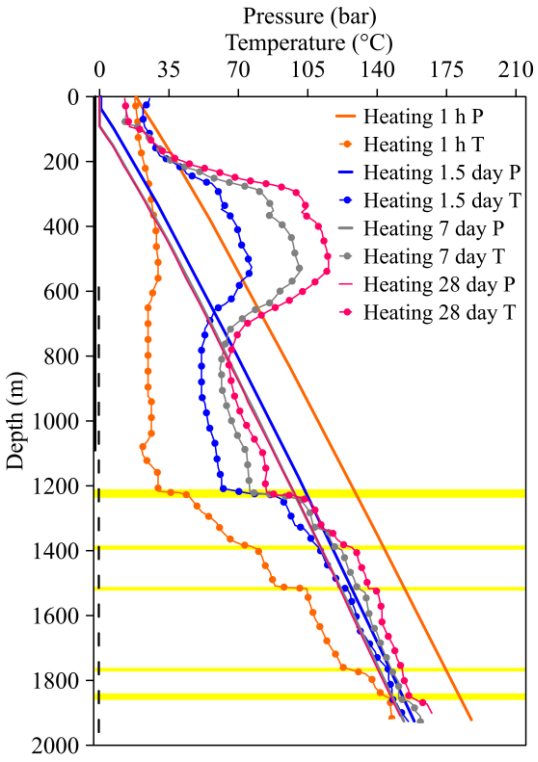

Figure 6: Well TH017 heat-up runs.

2.3. Numerical model

We employed McLean and Zarrouk's (2017) numerical modelling framework to examine pressure and temperature responses from geothermal well tests. The framework uses a grid geometry that consists of one vertical layer (Figure 7) with multiple blocks in the radial direction logarithmically spaced. The framework divides the elapsed time into various steps to match pressure, temperature, pressure derivative and temperature derivative while estimating the wellbore and reservoir parameters.

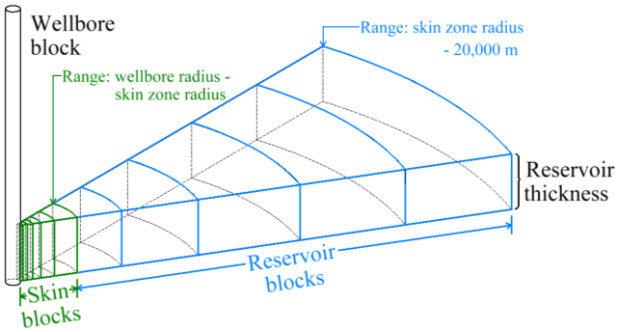

Figure 7: Grid geometry.

The McLean and Zarrouk (2017) framework utilises the fractional dimension to match the pressure response. We utilise an internal flow to match the temperature, in which the flow transports the heat from the reservoir into the wellbore. The internal flow rate and temperature change over time to match the temperature response.

Table 2 shows the parameters for the well TH017 numerical model. Wellbore volume, reservoir thickness, and wellbore

radius are the physical values from well TH017. The reservoir thickness (1144 m) runs from the 9 5/8" production casing shoe (1096 m) to the well TH017 bottom hole (2240 m). Injection temperature, skin zone, and permeability (calculated from type-curve matching) are input values for the numerical calculations.

Table 2: Well TH017 set-up parameters.

Parameter	Value
Well volume (m^3)	82
Well radius: r_w (m)	0.10795
Reservoir thickness: h (m)	1144
Model radial extent (km)	20
Skin zone blocks per layer	50
Reservoir blocks per layer	100
Injection temperature: T_{inj} (°C)	18.05
Skin zone radius: r_s (m)	5
Permeability: $k \times 10^{-15}$ (m^2)	3

2.4. Results

Zarrouk and McLean (2019) recommend avoiding zero flow for the pressure falloff period to suppress any existing internal flow. Also, the temperature profile can change rapidly, affecting the expansion of the fluid column and wireline. However, in this case, the temperature changes in the wellbore during the pressure falloff (at zero flow) are less than ~0.9°C (Figure 4). The temperatures before the target depth (1500 m) also show temperatures less than those for the target depth (Figure 6). There is also no indication of internal flows (Figure 6). Therefore, we analyse the pressure falloff of TH017 even when there is zero flow.

The model obtained good matches for the pressure and temperature (Figure 8). The fractional dimension is above 2.6 in the first 105 s of the pressure falloff period (Figure 8a). These fractional dimension numbers indicate that fluid enters the well from all directions, forming a sphere (3D-Flow). Next, at 105 s, the fractional dimension drops to 2.35, changing the major tendency from spherical to radial flow (2D-Flow) (Figure 8a). Afterwards, the fractional dimension sharply decreases to 1.77 (525 s).

At 525 s, the fractional dimension starts to drop gradually along the time up to the end of the pressure falloff period (Figure 8a). By the end (3925 s), the fractional dimension experienced a slight increase, reaching 1.66 (Figure 8a), indicating the tendency of fluid flowing radially from the reservoir to the wellbore is higher (2D-Flow).

The pressure drops gradually along the falloff period without reaching a stable pressure, although the TH017 pressure falloff period lasted 4060 s (1.13 hours) (Figure 8a), meaning low permeability (Zarrouk and McLean, 2019).

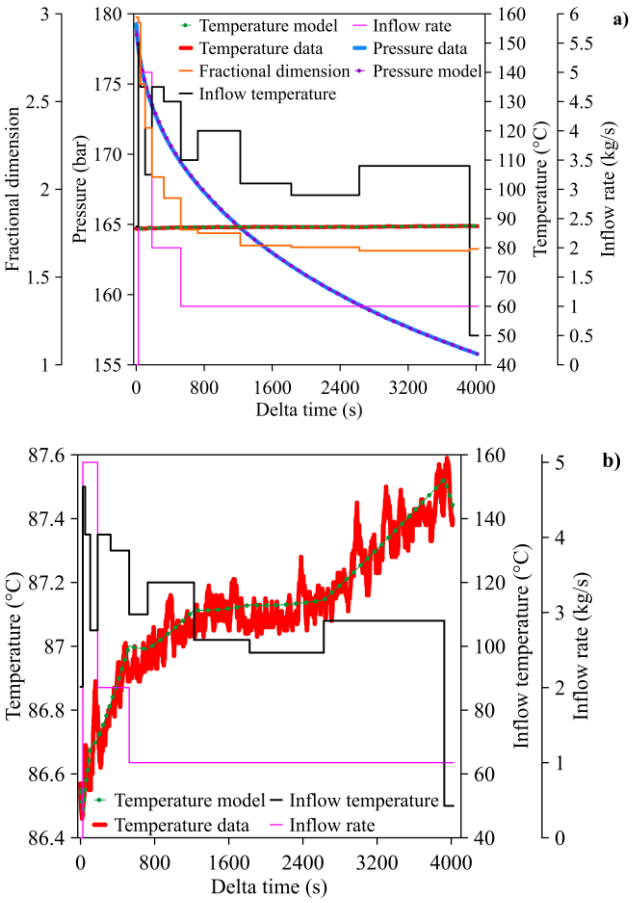

Figure 8: TH017 (a) pressure and (b) temperature match.

During the first 525 s, the temperature response showed the sharpest increase, changing from 86.56 to 86.89°C (Figure 8b). The inflow rate remains above 1.0 kg/s with inflow temperatures between 87.3°C and 150°C. This period shows the highest heat transfer interaction between the hot fluid and the injected water still travelling along the wellbore (Figure 8b).

Next, the temperature shows a period where it almost stabilises between 525 s and 2625 s, changing from 86.89°C to 87.15°C (Figure 8b). During this period, the inflow rate remains at 1.0 kg/s, while the inflow temperature rises at the beginning, followed by a continuous drop corresponding to the almost temperature stabilisation (Figure 8b). This period shows that the heat transfer interaction decreases because of the low permeability that prevents a higher hot fluid flow into the wellbore, prompting more dominance of the injected fluid over this period (Figure 8b).

After 2625 s, the temperature shows a steady linear increase, reaching a final temperature of 87.4°C (Figure 8b). Simultaneously, the inflow temperature increases, maintaining the same flow rate. This means a slight rise in the fluid flow from the reservoir and a decrease in the injected water effects (Figure 8b).

The temperature response shows short, sharp fluctuations throughout the pressure falloff period (Figure 8b) because the injected and hot fluids are still mixing. The temperature changes from 86.49 to 87.4°C (ΔT ~0.91°C), although the maximum temperature in well TH017 is 167.7°C (Figure 6), and the pressure falloff time is 4050 s. This minimal temperature increase indicates low permeability. The short

temperature fluctuations are also a sign of low permeability (Figure 8b).

The pressure derivative (Figure 9) shows features different from the standard pressure derivative (Zarrouk and McLean, 2019), with no development of a hump or reaching infinite acting pressure. In the first moments (<30 s), the pressure derivative shows multiple fluctuations without a wellbore storage effect. Then (>30 s), no hump appears, darkening the skin effects. Next (>300 s), the pressure derivative continues increasing linearly with a positive slope without clearly defined reservoir effects (Figure 9). Although the numerical model captures the pressure response, the first 30 s is challenging to match.

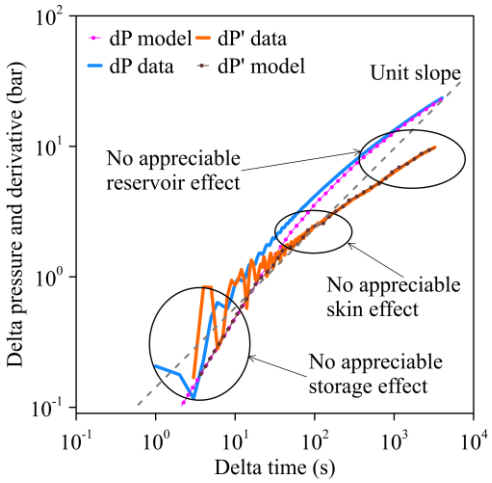

Figure 9: TH017 pressure derivative match.

The temperature derivative (Figure 10) lacks clear and defined paths and humps that indicate a smooth temperature rise or drop (Rangel-Arista et al., 2023). It shows fluctuations (short and significant) and gaps during the pressure falloff period (Figure 10). Before 10 s, the fluctuations are minor. After 10 s, the temperature derivative shows gaps and fluctuations (short and significant), indicating that an almost constant temperature was reached. The fluctuations become short after 2000 s, and the temperature derivative trend slightly increases (Figure 10). This can all be related to the small temperature changes/increase of about 0.5°C (Figure 8b).

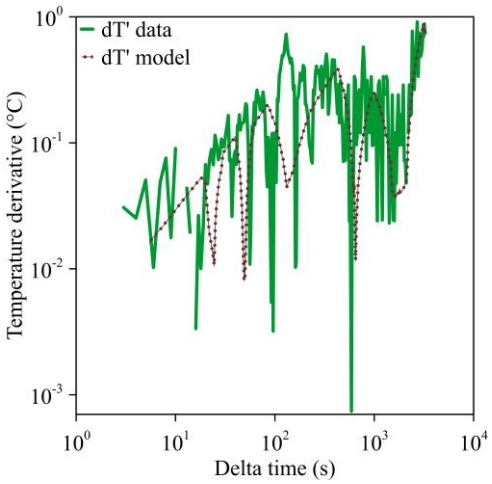

Figure 10: TH017 temperature derivative match.

By matching the pressure and temperature responses, we estimated the permeability, skin factor and skin zone permeability (Table 3). The estimated value for the reservoir and the skin zone also confirms the low permeability. The skin factor is positive, indicating possible damage to the wellbore during the drilling activities.

Table 3: TH017 parameters.

Parameter	Value
Injection temperature: T_{inj} (°C)	18.05
Skin zone radius: r_s (m)	3
Permeability: $k \times 10^{-15}$ (m^2)	1
Skin factor: s (dimensionless)	5
Skin zone permeability: k_s x 10^{-15} (m^2)	0.39

3. WELL WK684

Well WK684 belongs to the Wairakei geothermal field, New Zealand. This well encompasses a 30" conductor casing (0-36 m depth), 24" surface casing (0-154 m depth), 18 5/8" anchor casing (0-274.5 m depth), 9 5/8" production casing (0-596 m) and 7" liner (562.9-1193.3 m depth) (Figure 11). The open hole ranges from 596 to 1200 m (Figure 11).

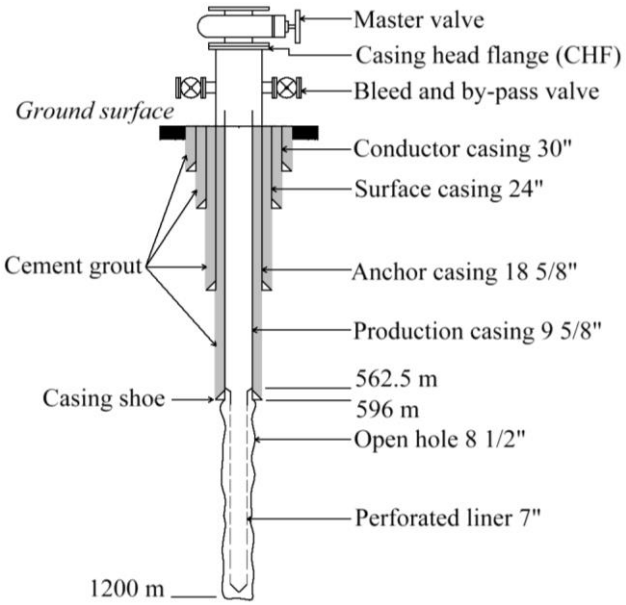

Figure 11: Well WK684 casing design.

3.1. Injection/falloff test

Well WK684 injection-falloff test uses decreasing flow injection steps. Initially, the sensor tool travels downward for 382 s (Point A), reaching a depth of 530 m and remaining at that point for 813 s (Figure 12, Point B). Next, at 1195 s (Point B), the sensor tool travels down and up between 530 and 1180.7 m depth up to 4653 s (Figure 12, Point C). During this period (Point B – Point C), the injection flow rate is 47.3 k/s. Likewise, the pressure and temperature fluctuate during this time because of the sensor tool movement.

After 7860.75 s (Point D), the sensor tool travels up and down to 11345 s (Figure 12, Point E). The pressure and temperature

ISSN 2703-4275

rise and drop, similar to the sensor tool movement. The injection flow rate remained at 31.5 kg/s (Figure 12, Point D – Point E).

At 11345 s (Point E), the sensor tool remains at 655 m up to 14112.25 s (Figure 12, Point F). A new injection step (15.8 kg/s) starts at 11441 s. The pressure and temperature experienced more appreciable falloff and buildup during this change of flow step, respectively (Figure 12, Point E – Point F).

After 14112.25 s (Point F), the sensor tool oscillates until 15426.25 s along the wellbore, reaching the target depth of 655 m by the end (Figure 12, Point G). The pressure and temperature responses show similar trends as the sensor tool movement. The 15.8 kg/s injection step lasts up to 15514 s.

During the three injection steps (47.3, 31.5, and 15.8 kg/s), the sensor tool also recorded the spinner velocity (Figure 13) while oscillating along the wellbore. The pressure profiles for the three injection steps show linear trends throughout the depth (Figure 13). The pressure profiles show lower values as the injection flow step drops, with the smallest pressure profile at 15.8 kg/s injection step and the highest at 47.3 kg/s injection step (Figure 13).

The temperature profiles for the three injection steps (47.3, 31.5, and 15.8 kg/s) show slight fluctuations from 524 to 670 m depth (Figure 13). Then, four sharp, short rises appear at 850, 995, 1152, and 1172 m. The temperature changes indicate possible feed zones (Figure 13, yellow bands). By the end (>1152 m), the temperature profiles reach 59.12°C (injection step: 15.8 kg/s), 59.03°C (injection step: 31.5 kg/s), and 58.59°C (injection step: 47.3 kg/s) (Figure 13).

The fluid velocity profiles show different trends for each injection flow step (Figure 13). The 15.8 kg/s velocity profile experiences a zero offset throughout the wellbore (Figure 13). The 47.3 and 31.5 kg/s velocity profiles show similar trends (Figure 13). From 524 to 620 m depth, the velocities fluctuate between 1.09 and 2.56 m/s (injection step: 47.3 kg/s) and 0.7 and 1.61 m/s (injection step: 31.5 kg/s). After the 620 m depth, the velocities drop continuously and become negative (684 m depth), showing a feed zone (Figure 13, yellow band). Then, both velocity profiles fluctuate close to zero throughout the period (Figure 13).

The temperature and velocity profiles (Figure 13) identified five possible feed zones (Table 4). The most significant feed zone runs from 620 to 684 m depth (Table 4).

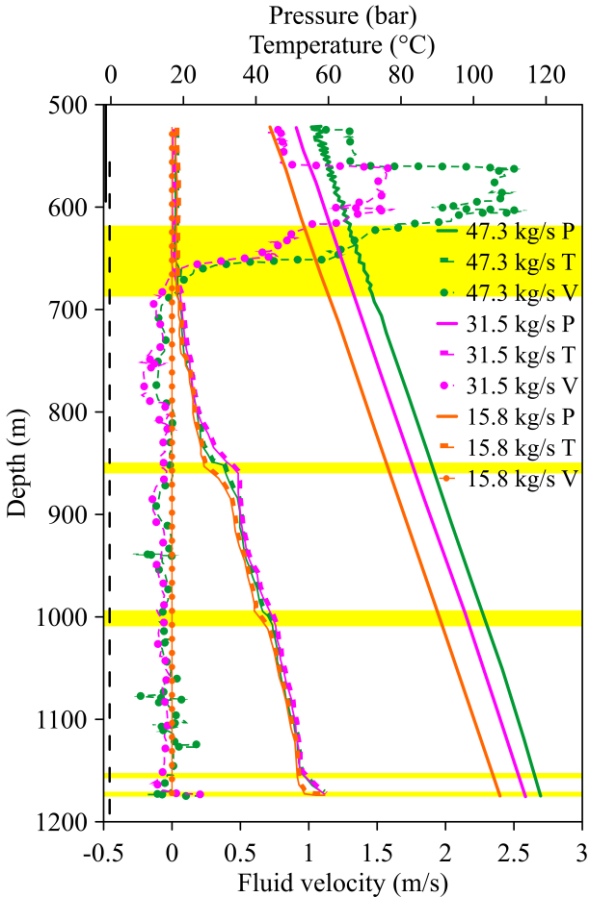

Figure 13: WK684 injection steps: pressure (P), temperature (T) and fluid velocity (V) profiles.

After the pressure, temperature, and velocity measurements during the three injection flow steps (47.3, 31.5, and 15.8 kg/s), the sensor tool reaches the target depth (655 m) at 15426.25 s (Figure 12, Point G). The 15.8 kg/s injection step lasts up to 15514 s.

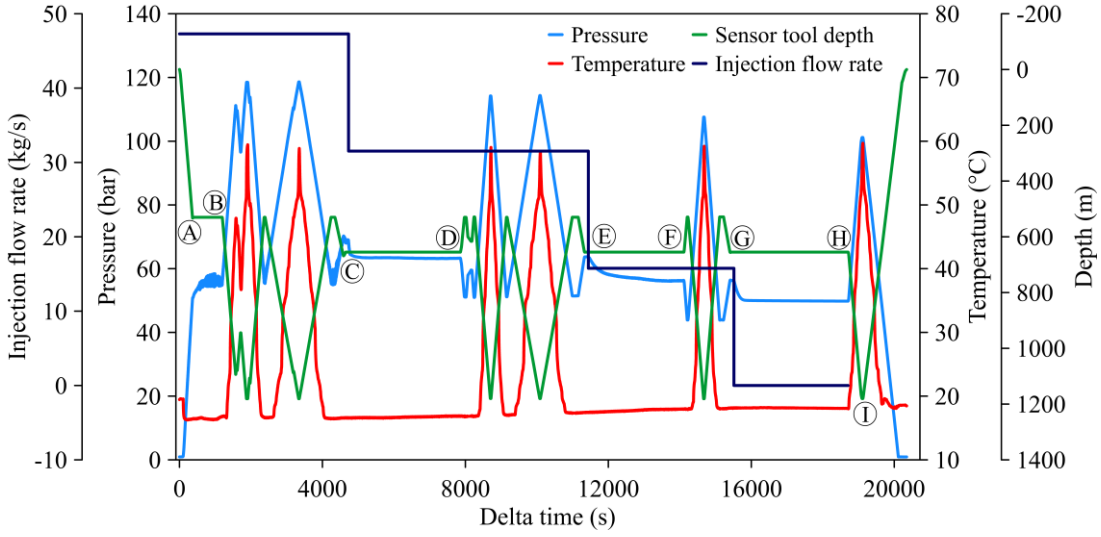

Figure 12: WK684 injection/falloff test.

ISSN 2703-4275

Table 4: Possible well WK684 feed zones.

Depth		Feed zone
From	To	
596	620	No
620	684	Yes
684	850	No
850	868	Yes
868	995	No
995	1010	Yes
1010	1152	No
1152	1158	Yes
1158	1170	No
1170	1175	Yes

At 15514 s (Figure 12), the injection flow step changes from 15.8 to 0 kg/s, commencing a non-flow falloff period. The sensor tool remained at the target depth (Figure 12). The pressure experienced a relative first rapid falloff from 56.27 to 50.09 bar in just 305 s (Figure 14). Then, the pressure goes into a second falloff, from 50.09 to 49.80 bar, for 2890.25 s.

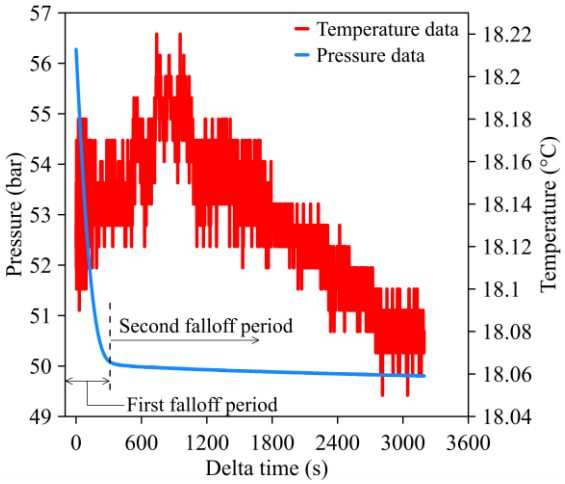

Figure 14: WK684 pressure falloff period: Pressure and temperature.

The temperature response shows minor fluctuations during the falloff period (Figure 14). Initially, the temperature starts at 18.13°C, reaching a maximum temperature of 18.22°C at two times: 740.25 s and 955.25 s. Then (>955.25 s), the temperature drops during the remaining time up to 18.08°C (Figure 14). The pressure falloff period lasts 3195.3 s.

After the pressure falloff time (>18709.75 s, Point H), the PTS tool travels downward to pass the test target to tag the deepest point of the well (1193.3 m) (Figure 12, Point I), which is a common practice in well testing (Zarrouk and McLean, 2019). Then, it travels upward to the ground surface. The pressure and temperature changed during this time because of the PTS tool depth variation (Figure 12). The well WK684 test lasted 20347 s (5.65 hours).

We calculated the injectivity index (II) for well WK684 at the target depth (655 m) (Figure 12), obtaining an II of 0.1 tonne/hr/bar (Figure 15).

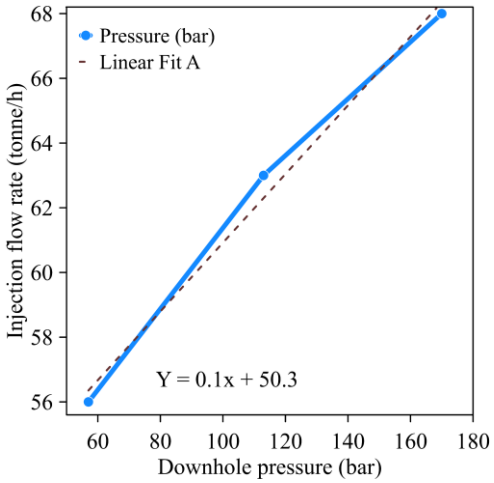

Figure 15: Well WK684 injectivity index (II).

3.2. Heat-up test

Well WK684 heat-up test recorded the pressure and temperature after 1 hour, 20 days and 48 days (Figure 16). The pressure profiles show that the pressure and the water well level decrease as time passes. By the end of the heat-up test (48-day pressure profile), the water well level stabilises above 200 m depth, and the maximum pressure reaches 97.25 bar (Figure 16).

Well WK684 possesses low permeability or a poor connection between the reservoir and the wellbore because the pressure control point (PCP) is absent (Figure 16) (Zarrouk and McLean, 2019).

The temperature profiles show the presence of two feed zones at 850 and 995 m depth (Figure 16, yellow bands), which are reaffirmed by the velocity and temperature profiles during the injection test (Figure 13, yellow bands).

ISSN 2703-4275

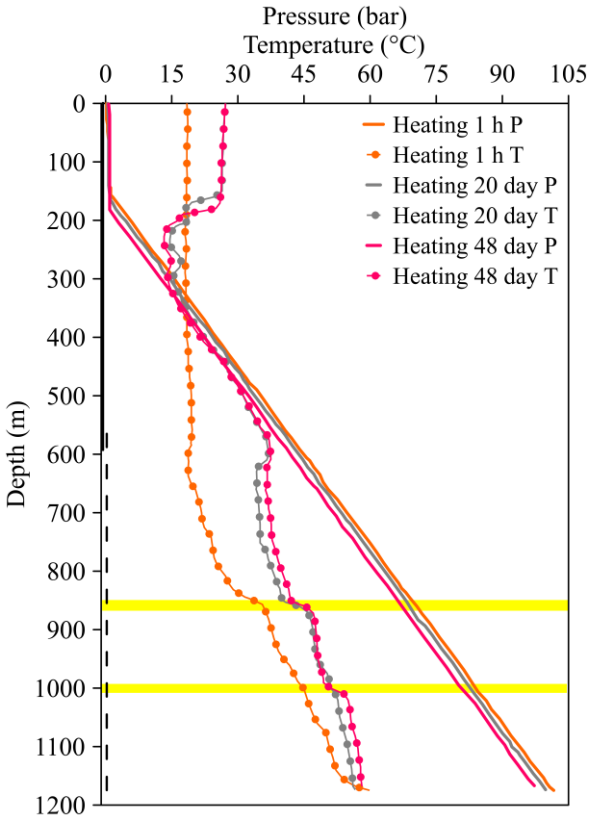

Figure 16: Well WK684 heat-up test.

3.3. Numerical model

To examine well WK684, we used the same framework and conditions described in section 2.3. Table 5 shows the parameters for the well WK684 numerical model.

Table 5: Well WK684 set-up parameters.

Parameter	Value
Well volume (m^3)	44
Well radius: r_w (m)	0.10795
Reservoir permeability: $k \times 10^{-15}$ (m^2)	3.7
Reservoir thickness: h (m)	604
Model radial extent (km)	20
Number of layers	1
Skin zone blocks per layer	50
Reservoir blocks per layer	100
Injection temperature: T_{inj} (°C)	18.05
Skin zone radius: r_s (m)	4

We estimated a permeability of 3.7 mD (Table 4) from the pressure falloff period of WK684 (Figure 14), employing the semilog pressure slope method (Figure 17) and Equation 1 (Zarrouk and McLean, 2019). The permeability value appears low but is a suitable initial value for modelling, which gave a permeability of 4 mD.

$$k = \frac{2.303qv}{4\pi mh} \quad (1)$$

Where k is the formation permeability (m^2), h is the reservoir thickness (m), q is the injection/production flow rate kg/s, v is the kinematic viscosity (m^2/s), m is the slope (Pa/log cycle).

3.4. Results

Although Zarrouk and McLean (2019) recommend avoiding zero flow for the pressure falloff period, we study this case because the temperature changes in the wellbore during the pressure falloff are less than ~0.17°C (Figure 14). The temperatures before the target depth (655 m) are below 37.48°C, and internal flows are absent (Figure 16).

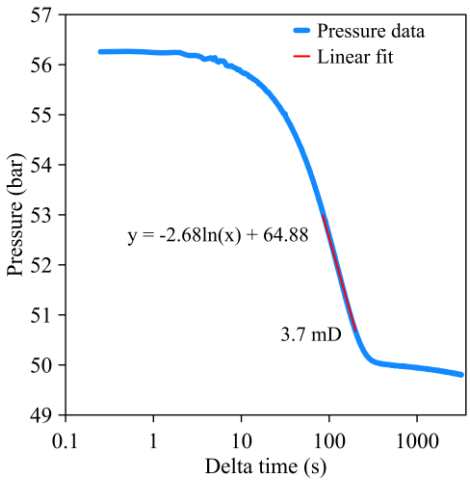

Figure 17: Well WK684 semilog pressure during falloff.

The model matches the pressure and temperature responses along the pressure falloff period (Figure 18). The fractional dimension remains at 2.45 in the first 15 s, meaning a higher trend of the fluid to flow radially (2-D flow). Next (>15 s), the fractional dimension increases up to 2.95 at 216 s, meaning a change in the flow trend from radial to spherical (3D-Flow) (Figure 18a).

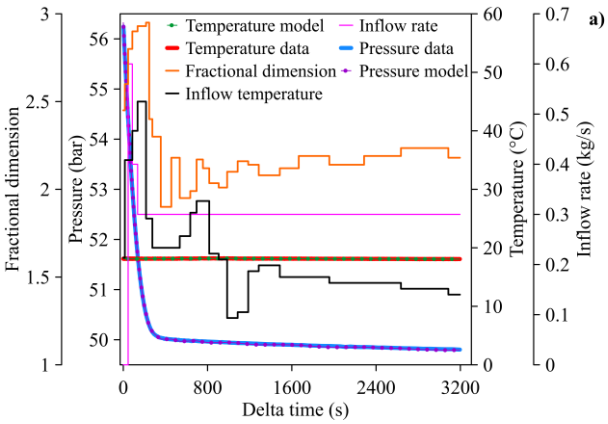

ISSN 2703-4275

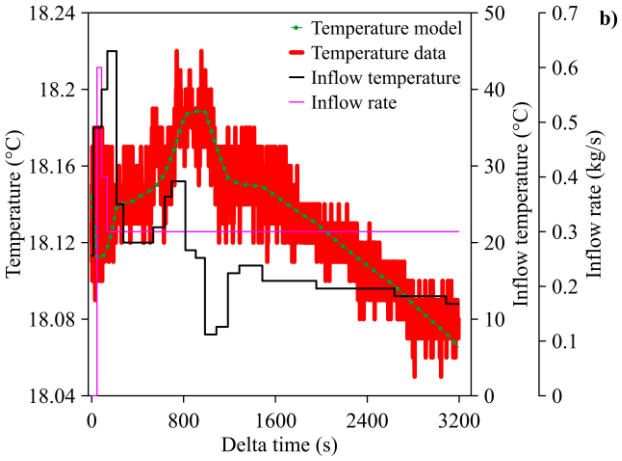

Figure 18: Well WK684 a) pressure and b) temperature matches.

Then, at 246 s (Figure 18a), the fractional dimension continuously drops, reaching 1.9 at 356 s—the fluid flow changes from spherical to radial (2D-Flow). Next, at 456 s (Figure 18a), the fractional dimension shows fluctuations around 2.13 up to the end of the pressure falloff period, indicating the fluid flows radially to the wellbore (2D-Flow). The fluctuations decrease as time passes, almost stabilising by the end at 2.18.

The inflow rate and temperature change show the most significant changes before 276 s because it is the period with the highest heat transfer interaction between the injected and hot fluids (Figure 8b). The heat transfer along the pressure falloff period is minor because the well WK684 shows temperatures less than 40°C at the target depth (655 m) and less than 60°C (highest recorded temperature) at the bottom (Figure 17).

The injected steps (Figure 12) quickly cool the wellbore and the nearby area (Figure 16). After the injection stops, the injected fluid still travels along the wellbore. However, heat transfer is insignificant because of the small temperature change and lack of considerable heat transfer (Figure 18b).

Although the heat transfer is minimal throughout the pressure falloff period, different times show slightly higher heat transfer interactions (Figure 18b). From 536 to 696 s, the inflow temperature rises from 20 to 28°C, while the inflow rate remains constant at 0.3 kg/s. This indicates an increase in heat transfer, prompting a very low rise in the temperature response. Then, at 816 s, the inflow temperature drops, reaching the lowest value (8°C) at 986 s. The temperature response shows sharp, short fluctuations without appreciable changes during the same period (Figure 18b). From 1086 to 1186 s (Figure 18b), the inflow temperature remains very low (9°C).

Afterwards (>1186 s), the inflow temperature suddenly increases and then gradually decreases until the end of the falloff period (Figure 18b). The temperature response slightly decreases with instant short fluctuations throughout the period (Figure 18b). The inflow rate remains constant during this period. This indicates a decreasing heat interaction between the injected and hot fluids, prompting a slight temperature decrease.

The model obtained a good pressure derivative match (Figure 19). In the beginning, the wellbore storage lasts for 10 s. Next, a defined hump appears that represents the skin effects. Afterwards, at 600 s, the pressure derivative shows a slope change, possibly indicating a boundary effect (Figure 19).

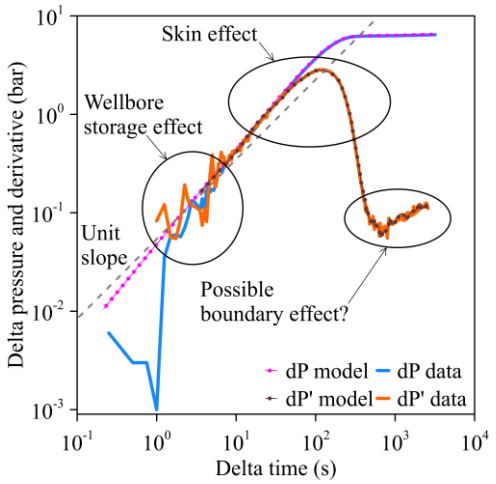

Figure 19: WK684 pressure derivative match.

The temperature derivative shows gaps and fluctuations (short and significant) throughout the period (Figure 20). The most prominent downward peaks represent an almost constant temperature, while the gaps represent the zones in which it was reached. Additionally, the temperature derivative lacks smooth and defined trends, indicating the absence of temperature rise (Figure 20). Although the model matches the pressure and temperature responses, the temperature derivative is challenging to match because of the instant fluctuations.

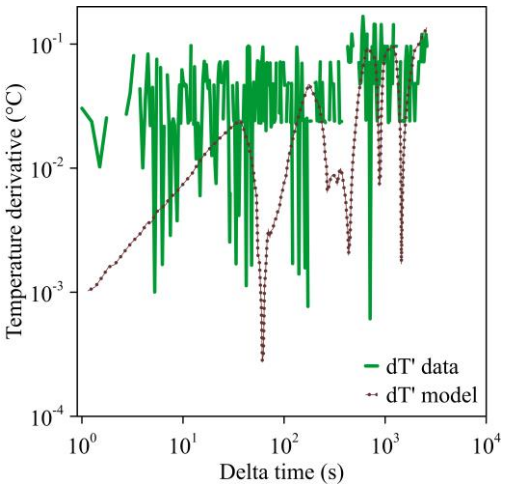

Figure 20: WK684 temperature derivative match.

By matching the pressure and temperature responses, the model estimated the parameters for well WK684 (Table 6). The permeability shows a value of 4 mD, which is low. The skin factor (-1) shows no damage in the near wellbore.

Table 6: WK684 reservoir parameters.

Parameter	Value
Skin zone radius: r_s (m)	4
Permeability: $k \times 10^{-15}$ (m^2)	4
Skin factor: s (dimensionless)	-1

ISSN 2703-4275

Skin zone permeability: $k_s \times 10^{-15}$ (m^2)	5.53

Although the temperature response remains almost constant, the pressure shows two defined falloff periods (Figure 14). However, the temperature response lacks stabilisation (Figures 14 and 16), showing multiple fluctuations throughout the period because of the low formation temperatures (<58°C).

4. CONCLUSIONS

The numerical modelling approach can match complex transient pressure and temperature responses while estimating the reservoir parameters for both cases (TH017 and WK684).

Overall, the TTA is an approach that can cast extra information about geothermal well tests and complement the analysis performed by the PTA. In this case, the temperature analysis helped confirm the existence of low permeability for both instances (TH017 and WK684) and the impact of low reservoir temperatures on temperature responses.

Although well TH017 is not a cold well (maximum temperature recorded 167.7°C). Still, the low permeability prevents a rapid heat transfer between the injected water and the inflow of hot fluid from the reservoir, prompting a prolonged temperature rise that took weeks to stabilise. The TTA showed the characteristic temperature response of wells with low permeability.

In the well WK684, the analysis helped to determine permeability (4 mD) and skin factor (-1). For the temperature response, there is no stabilisation because the well is cold, with temperatures less than 58.15°C, generating a small heat transfer interaction. Thus, a poor temperature buildup is not always related to low permeability. Cold temperatures in the wellbore can also trigger a poor temperature response.

The temperature derivatives with multiple gaps and short, sharp changes almost throughout the period indicate that the temperature fluctuates without stabilisation because of low permeability or cold wellbore temperatures.

ACKNOWLEDGEMENTS

The first author thanks the National Council of Humanities, Science and Technology of Mexico (CONAHCYT) for kindly providing the PhD scholarship to study at the University of Auckland.

This work was possible through the New Zealand Ministry of Business, Innovation and Employment (MBIE) through the Reversing Carbon Emissions in Geothermal Energy Industry – Template for Emissions – Intensive Industries project funds (UOAX2211).

The authors thank Contact Energy Ltd for kindly providing the data for this project.

NOMENCLATURE

h	is the reservoir thickness (m)
k	is the formation permeability (m^2)
k_s	is the skin zone permeability (m^2)
m	is the slope (Pa/log cycle)
q	is the injection/production flow rate kg/s
r_s	is the skin zone radius (m)
r_w	is the well radius (m)
s	is the skin factor (dimensionless)
T_{inj}	Injection temperature (°C)

Greek symbols

ν	Kinematic viscosity (m^2/s)

Acronyms

II	Injectivity index (tonne/h/bar)
WHP	Wellhead pressure (bar)

REFERENCES

Adiputro, A. S., Zarrouk, S. J., Clarke, R. J., Harcouët-Menou, V., Bos, S.: Geothermal wells with water hammer during injection falloff test: Numerical pressure transient analysis. *Geothermics* 2020, pp. 101838.

Dawkrajai, P., Yoshioka, K., Romero, A. A., Zhu, D., Hill, A. D., Lake, L. W. (2005). Annual report: A Comprehensive Statistically-Based Method to Interpret Real-Time Flowing Measurements. The University of Texas at Austin.

Grant, M. A., Bixley, P. F. (2011). Geothermal Reservoir Engineering. Elsevier.

Iyengumwena, R., Otutu, F., Yahaya, I., Ene, E., Yorkor, W., Fagbami, D. (2013). Perforating multiple sands with long interval separations pushes the limit in completion efficiency. In: *IPTC 2013: International Petroleum Technology Conference, Beijing, China*.

Mclean, K., Zarrouk, S.: Pressure transient analysis of geothermal wells: A framework for numerical modelling. *Journal of Renewable Energy 2017*. pp. 737-746.

Onur, M., Palabiyik, Y. (2015). Nonlinear parameter estimation based on history matching of temperature measurements for single-phase liquid-water geothermal reservoirs. In: *World Geothermal Congress, Melbourne, Australia*.

Panini, F., Onur, M. (2018). Parameter estimation from sandface drawdown temperature transient data in the presence of a skin zone near the wellbore. In: *SPE Europec Featured at 80th EAGE Conference and Exhibition, Copenhagen, Denmark*.

Ramazanov, A. S., Parshin, A. V.: Temperature distribution in oil and water saturated reservoir with account of oil degassing. *Oil Gas Business Journal 2006.* pp. 1–16

Rangel-Arista, J.A., Zarrouk, S.J., Kaya, E., McLean, K. (2022). Exploring the Use of Temperature Transient Analysis During Pressure Falloff Testing in Geothermal Wells. *44th New Zealand Geothermal Workshop, Auckland, New Zealand*.

Silva Junior, M. F., Muradov, K., Carvalho, M. S. (2012). Modelling and Analysis of Temperature Transients Caused by Step-Like Change of Downhole Flow Control Device Flow Area. In: *the SPE Latin American and Caribbean Petroleum Engineering Conference, Mexico City, Mexico*.

Sui, W., Zhu, D., Hill, A.D., Ehlig-Economides, C.A. (2008). Model for Transient Temperature and Pressure Behavior in Commingled Vertical Wells. *The 2008 SPE Russian Oil & Gas Technical Conference and Exhibition, Moscow, Russia*.

Zarrouk, S.J., McLean, K. (2019). Geothermal well test analysis: fundamentals, applications and advanced techniques. Elsevier.

ISSN 2703-4275